The challenge of using the W band in satellite communication

C. Riva[1,2,*,†], C. Capsoni[1,2], L. Luini[1], M. Luccini[1], R. Nebuloni[2] and A. Martellucci[3]

[1]DEIB – Dipartimento di Elettronica, Informazione e Bioingegneria, Politecnico di Milano, Piazza L. Da Vinci 32
20133 Milano, Italy
[2]CNR – IEIIT, Via Ponzio 34/5, 20133 Milano, Italy
[3]TEC-EEP, ESA/ESTEC, Noordwijk, The Netherlands

1. INTRODUCTION

Satellite and terrestrial telecommunication (TLC) systems greatly benefit from the use of very high frequency bands, the main advantages being the availability of larger bandwidths and the smaller antenna size for a fixed gain. Moreover, the possibility of using on-board antennas with enhanced directivity is attractive for satellite systems whose coverage area is subdivided in spot beams for frequency reallocation or regional services. A clear statement of the interest in using the W band is the decision of the Federal Communications Commission of the USA 'to promote non-Federal Government development and use of the 'millimeter wave' spectrum in the 71–76 GHz, 81–86 GHz and 92–95 GHz bands on a shared basis with Federal Government operations. These bands are available for use in a broad range of new products and services, including high-speed, point-to-point wireless local area networks and broadband Internet access. Highly directional, 'pencil-beam' transmissions can be engineered in close proximity to one another without causing interference'. The W band is attractive for space systems, including fixed satellite services and space exploration missions. In particular for the case of a geostationary High Throughput System providing multimedia service to the user link at Ka band [1], the use of W band for the feeder link (i.e. large available bandwidth) could reduce significantly the number of gateways with respect to Ka and Q/V bands, thus permitting a simpler exploitation of the smart gateway concept [2] (i.e. the dynamic rerouting to another gateway of the traffic from a station unavailable because of failures or excessive attenuation). For deep space missions, the main driver for the interest in using the W band is the possible increase in the on-board antenna gain with respect to the values at X and K bands considered for current or planned missions.

*Correspondence to: C. Riva, DEIB – Dipartimento di Elettronica, Informazione e Bioingegneria, Politecnico di Milano, Piazza L. Da Vinci 32, 20133 Milano, Italy.
†E-mail: riva@elet.polimi.it

The drawback of using radio waves at frequencies in Q/V and W bands is the definite impact of the impairments caused by the troposphere as evidenced in [3–6].

As a consequence, the design of TLC systems at Q/V and W bands, and in particular satellite based ones, cannot rely on the classical approach of simply assigning an extra power margin to counteract atmospheric fades. The extensive use of Fade Mitigation Techniques (FMTs), such as link power control, site diversity or on board adaptive power allocation, from the propagation side, adaptive coding and modulation and data rate adaptation, from the telecommunication side, is mandatory [7]. A reduction of the QoS should also be considered.

This contribution reviews the propagation impairments caused by the troposphere and, for each of them, evidences of the characteristics and the modelling issues in the W band. In Section 2, the tropospheric effects in non-precipitating atmosphere are described, while in Section 3 the attenuation due to rain is discussed. Section 4 deals with depolarization and scintillations, and Section 5 presents some considerations about the design of TLC systems operating in the W band. Finally, Section 6 draws some conclusions.

2. GASES AND CLOUDS

While at Ku band rain plays the prevailing role among the tropospheric impairments, at Ka band and above, also the effects due to gases and clouds must be considered, especially in the design of middle and low availability systems [8]. Oxygen and water vapour are practically the only gaseous components affecting the electromagnetic wave propagation in the 20–300 GHz frequency range.

Oxygen attenuation, being weakly dependent on ground temperature and atmospheric pressure, is relatively stable in time (during the day, the month and the year) and in space (it varies slightly across the globe). On the other hand, its dependence on frequency is much stronger due to the resonant absorption band of the oxygen molecules, the specific attenuation exceeds 10 dB/km at 60 GHz (hence, any Earth-satellite link is unfeasible because of the tropospheric effects, while the use of the 60 GHz band is envisaged for inter-satellite links), whereas decreases from about 0.26 dB/km down to about 0.02 dB/km between 70 and 95 GHz in the W band [9]. Differently from the one of oxygen, the water vapour attenuation, being a function of temperature, pressure and humidity, is characterized by marked daily, seasonal and geographical variations. Water vapour specific attenuation exhibits a broadened peak around the H_2O absorption line at 22.2 GHz, whilst it increases monotonically in the 40–100 GHz interval and, in the W band (70–95 GHz), is comprised between 0.24 and 0.43 dB/km at mean sea level reference conditions (temperature 15°C, pressure 1013 hPa and water vapour density 7.5 g/m^3) [9].

Because of the opposite dependence of oxygen and water vapour attenuation on frequency, the specific gas attenuation (i.e. because of oxygen and water vapour) in the W band, in reference conditions, is comprised between 0.36 and 0.5 dB/km, being higher at the bandwidth edges (70 and 95 GHz) and lower in the centre, as shown in Figure 1 [9]. Then the total gaseous attenuation along the slant path will depend on the actual distribution of air temperature, humidity and total pressure; just as an example, the predicted [9] zenith gas attenuation exceeding 1% of the time at 80 GHz ranges between 1 and 3 dB almost all over the globe [8].

The models currently recommended by the International Telecommunication Union – Radiocommunication (ITU-R) sector for the prediction of gaseous attenuation along a slant path [9] rely on solid physical bases and, as such, they are expected to provide reliable estimations at least up to 100 GHz. Such models introduce simplified (yet accurate) formulations relying on effective parameters, like the oxygen effective height (analytical function of frequency and pressure) and the water vapour total content (global maps of this parameter are available in [10], and its accuracy has been evaluated in [11]), which embed information on the vertical profiles of oxygen and water vapour
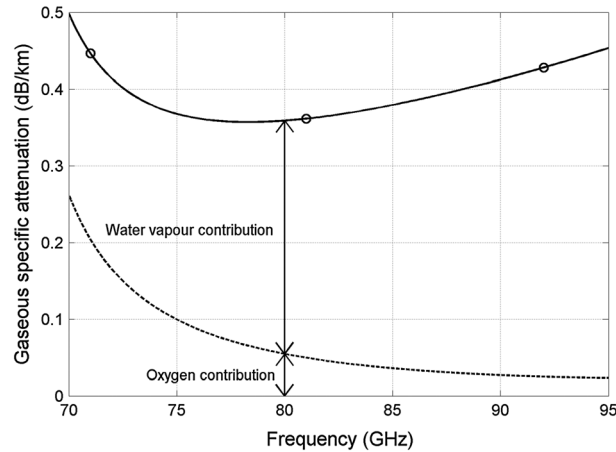
Figure 1. Gas (oxygen and water vapour) specific attenuation (dB/km) as a function of frequency (GHz) in reference conditions (temperature 15°C, pressure 1013 hPa, water vapour density 7.5 g/m3); circles correspond to the center frequencies of 71, 81 and 92 GHz. The separate contributions due to oxygen and water vapour are evidenced.

concentrations. The mean yearly distribution of oxygen and water vapour zenith attenuation is calculated by multiplying their specific attenuation in reference conditions by the effective parameters. As a final step, the slant path attenuation is obtained through the cosecant law, under the plausible assumption of local homogeneity of the atmosphere. If local input radio-climatological parameters are not available, then the ITU-R recommends to use maps, which have been derived from the ERA-40 product generated by the European Centre for Medium-Range Weather Forecasts using a Numerical Weather Prediction (NWP) system [12].

Because the ITU-R models [9] have been validated for frequencies only up to 50 GHz [13], further validation is recommended before their use for system design in W band, even though their good performance is not expected to decrease substantially.

The accuracy of the ITU-R models can be assessed by using as reference (namely 'measurements') the attenuation calculated by integrating along the path the gaseous specific attenuation, which, in turn, can be derived with great accuracy by physical spectroscopy models of air refractivity, such as those provided by Liebe [14, 15] and Rosenkranz [16]. A comprehensive summary of the currently available physical models of the atmosphere can be found in [17]. This approach obviously requires the availability of vertical profiles of water vapour and oxygen concentration as inputs to such models, which are provided by radiosonde observations (RAOBS) such as the Fondazione Ugo Bordoni – European Space Agency radiosoundings (FERAS) database that includes vertical profiles of pressure, humidity and temperature (PHT) collected twice a day for 10 years (1980–1989) in non-rainy conditions, in several sites worldwide [18]. We have selected two FERAS sites in Europe with different climatic features: Madrid (Spain, lat. 40.47°N, long. −3.57°E, alt. 600 m a.m.s.l.) and Spino d'Adda (Italy, lat. 45.4°N, long. 9.5°E, alt. 84 m a.m.s.l.). Figure 2 shows the complementary cumulative distribution functions (CCDFs) of gaseous zenith attenuation for the two sites at 71 (upper curves) and 81 GHz (lower curves), calculated in one case by integrating along the path the results of the Liebe MPM93 model [15], fed with local FERAS radiosonde data, and in the other case by using the ITU-R recommendations [9] fed with ITU-R input climatological maps. Indeed, the ITU-R maps are derived from an NWP system (i.e. ERA-40), which assimilates, among the others, also radiosonde data into a global atmospheric model. Therefore, radiosonde and ITU-R maps are not strictly independent, however, validation performed at sites equipped with independent ground remote sensing instruments for water vapour and cloud liquid content (i.e. microwave radiometer (MWR)) confirmed that RAOBS are in good agreement with MWR observations up to 5% of the annual time [11]. Therefore, even if it is of course not possible to draw general conclusions from the examples shown in Figure 2, it is evident that the ITU-R predictions are quite accurate. We can notice that at 1% of the yearly time (system availability of 99%), the fade margin due to gases is between 1.2 and 2.1 dB in the 71–81 GHz band. It is worth noting that, since 1% is the lowest time percentage to be
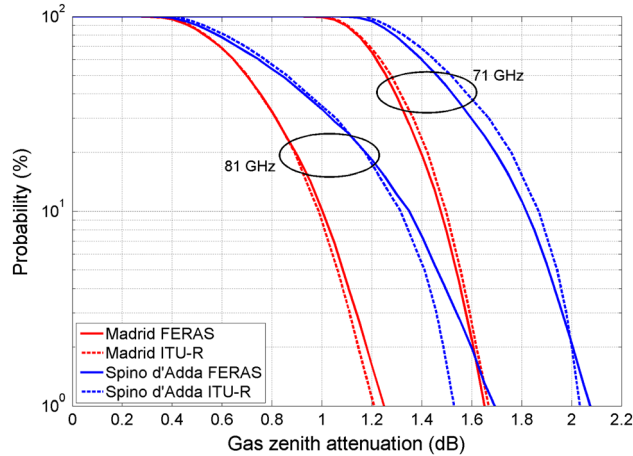
Figure 2. Complementary cumulative distribution functions of zenith gaseous (oxygen and water vapour) attenuation calculated by integrating 10 years of Fondazione Ugo Bordoni – European Space Agency radiosoundings vertical pressure, humidity and temperature profiles for Madrid (red solid line) and Spino d'Adda (blue solid line), at 71 GHz (upper curves) and 81 GHz (lower curves); the corresponding ITU-R models predictions are shown as dashed lines with the same colours.

considered for gas (and cloud) attenuation in the method for the combination of the effects in [19], the gas attenuation at 1% is the maximum value to be taken into account in the link margin calculation.

In non-precipitating atmosphere, another key impairment to be definitely taken into account is the attenuation due to clouds. Because in the W band, the size of suspended water droplets in clouds is smaller than the wavelength, the Rayleigh approximation can be used for the computation of the extinction cross sections and, thus, the cloud attenuation depends only on the liquid water content, on the droplets temperature and, obviously, on the frequency. Cloud attenuation is highly variable, depending on the presence of clouds along the link and on their liquid water content; it is monotonically increasing with frequency in the 10–100 GHz band. Moreover, cloud attenuation markedly depends on climate.

In ITU-R recommendation P.840-5 [20], cloud attenuation is calculated through an effective parameter, that is, the reduced liquid water total content measured in kg/m^2 or mm. This parameter is a function of frequency, and its statistics are currently calculated by ITU-R in the 20–50 GHz band (but it can be recalculated in different frequency bands) and distributed through global maps [11, 20]. Cloud attenuation is then obtained as a function of the reduced liquid water total content, the water permittivity, the frequency and the elevation angle. As for gases, physical models of clouds, coupled with radiosonde observations, represent the most accurate way to assess the accuracy of the prediction models. However, because radiosoundings do not measure directly the cloud water content, a cloud detection algorithm is required to identify cloud layers and to estimate the cloud water content from PHT vertical profiles. Also in this case, as for gaseous attenuation, the comparison between measurements of the cloud liquid provided by RAOBS data and MWR observations at selected sites confirmed the possibility to use RAOBS data to validate ITU-R maps derived from NWP products [11].

Figure 3 shows the CCDFs of cloud zenith attenuation for Madrid and Spino d'Adda at 91 GHz, predicted by ITU-R models [20]. The CCDFs calculated using FERAS radiosonde data, by coupling the Helsinki University of Technology model [21] (modified as reported in [22]) and the Liebe MPM93 mass absorption model [15], are shown for comparison. The above mentioned cloud detection model is the one actually selected by the ITU-R, and its validity and applicability range has been fully investigated in [22]. From the few examples shown in Figure 3, it is clear that the ITU-R model in recommendation P.840-5 tends to overestimate cloud attenuation, which may be partially ascribable to the reduced liquid water content calculated in the 20–50 GHz band. Indeed, the accurate estimate of the liquid water content in the atmosphere is still an issue.

For the considered sites, the zenith fade margin due to clouds for an outage probability of 1% (system availability of 99%), falls between 3 and 4 dB in the W band, that are, as recalled for gas attenuation, the maximum cloud contribution to be considered in [19] to calculate the total fade margin.
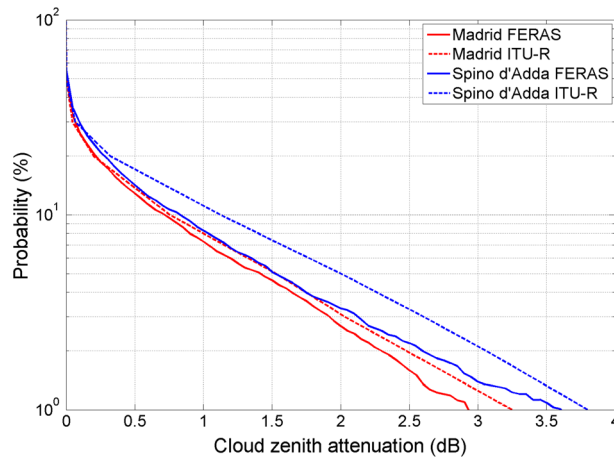
Figure 3. Complementary cumulative distribution functions of zenith cloud attenuation calculated by integrating 10 years of Fondazione Ugo Bordoni – European Space Agency vertical pressure, humidity and temperature profiles for Madrid (red solid line) and Spino d'Adda (blue solid line), at 91 GHz; the corresponding ITU-R models predictions are shown as dashed lines with the same colours.

Figure 4 shows the CCDFs (solid lines) of oxygen, gas (oxygen and water vapour) and gas and cloud zenith attenuation calculated by integrating 10 years of FERAS vertical PHT profiles for Spino d'Adda, at 81 GHz; the corresponding ITU-R models (dashed lines) predictions are also shown for comparisons. Considering an outage probability of 1%, where usually also a rain contribution to attenuation has to be added being the probability of rain typically in the range 5–10%, the fade margin associated to non-precipitating atmosphere for Spino d'Adda at the zenith is about 4.75 dB in the W band; about 0.25 dB is due to the oxygen, 1.5 dB to the water vapour and 3 dB is due to cloud.

3. RAIN

At frequencies higher than 10 GHz, the wavelength becomes comparable to the size of hydrometeors (few millimetres), which absorb and scatter part of the incident electromagnetic energy, causing significant signal fades. The amount of rain attenuation affecting Earth-to-satellite links is obtained
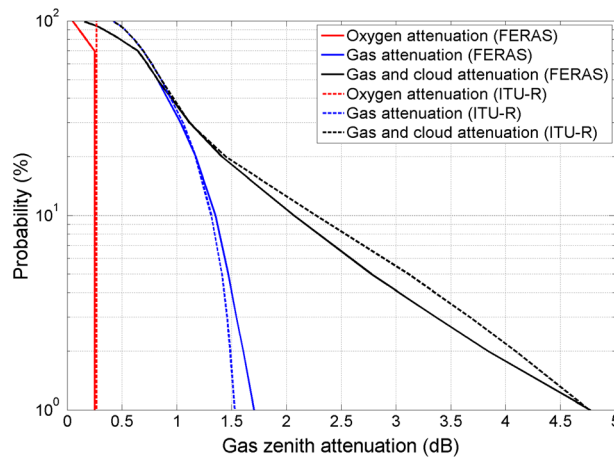
Figure 4. Complementary cumulative distribution functions of oxygen (red solid line), gas – oxygen and water vapour – (blue solid line) and gas and cloud (black solid line) zenith attenuation calculated by integrating 10 years of Fondazione Ugo Bordoni – European Space Agency radiosoundings vertical pressure, humidity and temperature profiles for Spino d'Adda, at 81 GHz; the corresponding ITU-R models predictions are shown as dashed lines with the same colours.

by integrating along the path of the specific attenuation, the latter being dependent on the rain intensity R (mm/h) as follows:

$$\gamma_R = k R^\alpha \qquad (1)$$

In (1), k and α are coefficients (provided for instance in recommendation ITU-R P.838-3 [23]) for statistical computations, which depend on the frequency, elevation angle, drop temperature, wave polarization (as raindrops are not spherical), drop size distribution (DSD) and shape. Indeed, marked differences in the specific rain attenuation come from the variation of the DSD that may occur from event to event and, sometimes, also during the same event. As an example, Figure 5 shows the relationship between the rain intensity and the specific attenuation at 81 GHz in horizontal polarization (the more attenuated one) along a 37.7° slant path: each curve in the figure originates from a different gamma DSD. Raindrops have been modelled as oblate spheroids [24], and the Fredholm Integral equation Method (FIM) method [25] has been used for the calculation. At frequencies in the W band, the effect of the DSD is more definite than in the lower bands, with a marked dependence on the rain intensity: at 10 mm/h, the peak to peak relative variation in the specific attenuation is about 40% (for both polarizations). The difference between specific attenuation in vertical and horizontal polarization is well below 5%. This issue has to be considered when applying instantaneous frequency scaling algorithms in uplink power control mitigation technique. As for the prediction of local attenuation CCDF, the authors assume it is convenient to make reference to the κ and α coefficients proposed by ITU-R in [23] in order to avoid confusion. Nevertheless, they would like to stress that the aforementioned figures originate from a best fitting procedure and their full appropriateness to the W band is still to be verified.

The CCDF of rain attenuation is directly related to the local rain rate CCDF, which may vary significantly from site to site; as an example, Figure 6 shows the rain rate distributions relative to the European sites already considered in the previous section (namely Madrid and Spino d'Adda), as estimated by recommendation ITU-R P.837-6 [26]: the difference between the curves (e.g. considering Madrid and Spino d'Adda, a relative rain rate variation of approximately 35% is expected at $P = 0.01\%$ of the yearly time, which corresponds approximately to 1 hour in a year) is ascribable both to the mean yearly number of rain events affecting the two sites and to their intensity. In this respect, the knowledge of the rain rate CCDF is of key importance because the probability to have rain, referred to as P_0, is very close to P_A, the probability to have rain attenuation (typically, for temperate climate $P_0 \approx 4$–8% [26], and $P_A \approx 6$–10%, depending on the link elevation angle).

In the last three decades, considerable research efforts have been addressed to the development of models aimed at predicting rain attenuation statistics from the knowledge of the CCDF of the local rainfall intensity. Several methods have been developed, and recently, their performance was evaluated against direct measurements in the 17–50 GHz range [13], included in the DBSG3 experimental
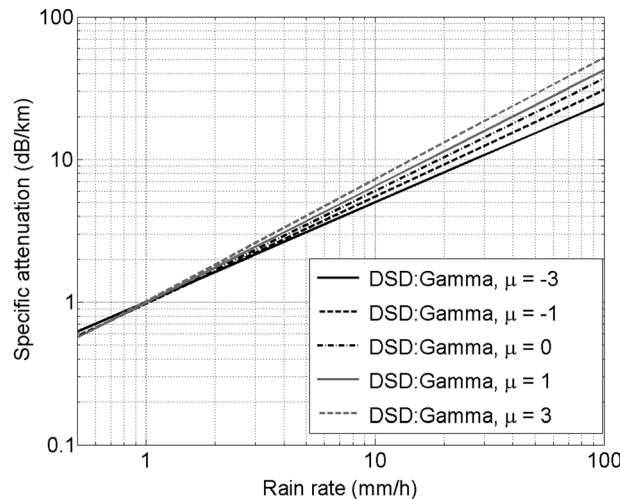
Figure 5. Specific rain attenuation (dB/km) at 81 GHz (for horizontal polarization and link elevation of 37.7°) as a function of rain rate (mm/h) for several drop size distribution models.
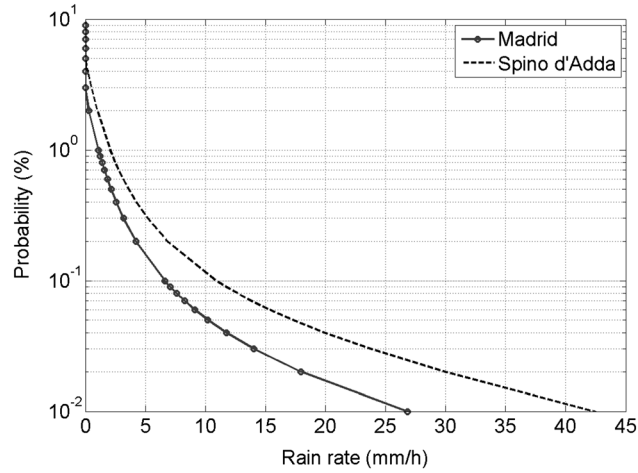
Figure 6. Complementary cumulative distribution functions of rain rate for Madrid (solid line with circles) and Spino d'Adda (dashed line); predictions according to recommendation ITU-R P.837-6.

database made available by the ITU-R [27], providing overall satisfactory results. Because no experimental measurements are available for Earth-to-satellite links at frequencies above 50 GHz against which the models' performance could be tested, methods developed on solid physical bases should be preferred, as their estimation accuracy is not expected to depend markedly on the frequency. In this scenario, the SC EXCELL (Stratiform Convective EXponential CELL) [28] model represents one of the privileged candidates because of its physical nature (which allows its easy extension also to terrestrial radio links [29]) and its very good overall prediction performance [13]. It describes the meteorological environment as an ensemble of synthetic isolated rain cells, in which the spatial distribution of the rain intensity is modelled with a decaying exponential function; moreover, SC EXCELL takes separately into account the contribution to attenuation due to stratiform and to convective rain (i.e. different rain height and different rain intensity). Finally, the contribution due to the melting layer is added only to stratiform rain as an equivalent rain slab whose height depends markedly on frequency. Empirical methods, whose parameters are usually derived from the comparison with measurements, are less attractive in this context because they are not adequately 'tested' against measurements in the W band.

An example of the application of rain attenuation models is provided in Figure 7, which depicts the CCDFs of slant path rain attenuation (Madrid, frequency = 81 GHz, satellite orbital position = 16°E, link elevation = 39° and vertical wave polarization) as predicted by the SC EXCELL model and by
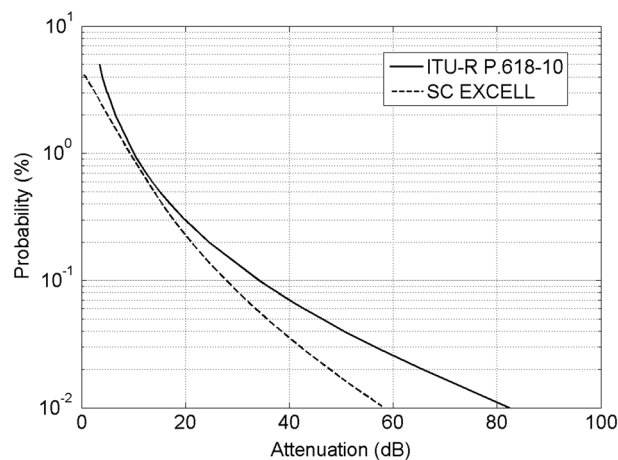
Figure 7. Complementary cumulative distribution functions of rain attenuation at 81 GHz for Madrid, Spain (lat. 40.47°N, long. −3.57°E, alt. 600 m a.m.s.l.) along a 39° slant path; predictions using the ITU-R P.618-10 (solid line) and SC EXCELL (dashed line).

the model included in recommendation ITU-R P.618-10 [19], which is the current reference semi-empirical method for rain attenuation prediction. Figure 7 clearly indicates a huge variability in the prediction of the rain attenuation statistics obtained at 81 GHz from the two models (e.g. more than 20 dB for $P = 0.01\%$), which, on the other side, provide quite similar results in the 17–50 GHz band [13]. This finding definitely points out the need of a reliable measurement data set for the development/assessment of rain attenuation models at frequencies higher than 50 GHz. Indeed, additional research efforts are still required to reliably predict rain attenuation at frequencies above the V band: from the experimental side, advanced propagation instruments and more refined methodologies to acquire and process attenuation data are crucial to improve the quality of the reference measurements, whilst from the theoretical side, it is necessary to improve the models' prediction accuracy especially at high yearly time percentages, which correspond to fade levels that can be counteracted. Moreover, measurements of path attenuation at multiple frequencies and sites, together with radiometric measurements, have to be strongly encouraged. As for the other 'ingredients' to predict the attenuation CCDF, that is, the input $P(R)$ and the κ and α coefficients to convert rain rate into specific attenuation, they appear, in some respect, to be less critical. Different techniques to predict/derive long-term $P(R)$ are nowadays available among which to choose the most appropriate one for the site of interest (according on the available local information) [26, 30, 31]; on the contrary, the open problem is how to correctly describe the year-to-year variability (risk assessment). The rain rate to specific attenuation conversion is in general a very big issue for the radar meteorology community. In propagation applications, the DSD variability from event to event and sometimes within the same event, impacts on the instantaneous frequency scaling, but the average relationships, although partially dependent on the geographical/meteorological region, are well established.

4. SCINTILLATION AND DEPOLARIZATION

Tropospheric scintillation is due to small-scale refractive index non-homogeneities induced by atmospheric turbulence along the propagation path. As a result, rapid fluctuations of the received signal amplitude affect satellite links above about 10 GHz. The intensity of tropospheric scintillation is usually quantified in terms of the signal standard deviation calculated during a stationary period of few minutes, which depends on the turbulence structure index, increases with the frequency (but much less than rain attenuation) [32] and with the path length and decreases when the antenna size increases because of aperture averaging. Scintillation can be due also to the variation of the arrival angle of the main ray, which increases when the beamwidth decreases as a result of the effect of the antenna radiation pattern [32]. The impact of scintillation on the fade margin calculation is quite limited with respect to attenuation, at least for high availability systems and elevation angles above 15°, but it can be important for low elevation angles and low margin systems. If only gateways are considered, the dominant effect remains attenuation but scintillation due to angle of arrival variations must be considered for large antennas and high frequencies because they scale as the square power of frequency [32]. Moreover, it is worth noting that the dynamics of scintillation may interfere with tracking systems or fade mitigation techniques. The present model recommended by ITU-R [19] is applicable up to a frequency of at least 20 GHz, but it has been noticed [32] that it is not in very good agreement with measurements at various sites at Ka and Q/V bands (up to 50 GHz), possibly due to the variation of the angle of arrival of the main signal, which likely play a role for highly directive antennas (as in the case of very high frequencies). The relative impact of angle-of-arrival fluctuations on measured scintillations requires further study. Scintillation can also occur inside rain and, in this case, they are mixed with the fast fluctuations induced by rain itself. A model based on a theoretical approach, using Tatarskii's theory [33] of scintillation in clear sky, has been proposed and tested for different sites and frequency up to V band [34]. Scintillation, apart from their impact on the performance of communications systems (especially those with low-margin) [35], may interfere with tracking systems or FMT. The scintillation effects at W band require an experimental assessment due to the very narrow antenna beamwidth.

If the use of dual polarization is foreseen, the depolarization (specifically, cross polarization discrimination - XPD) introduced by the non-spherical particles (drops and ice crystals) must be taken into account. In particular, the physical parameters that cause XPD are the anisotropy (i.e. the polarization-dependent forward scattering of the particles) and the angle of the symmetry axes of the particles with respect to the polarization plane (canting angle). In [36], it is shown that depolarization at a given frequency can be scaled to a different one by scaling the corresponding anisotropies.

The hydrometeor axes, however, are not equi-aligned, and the dispersion of these orientations is, generally, beneficial (reduce) to XPD, although the phenomenon becomes much more complex and difficult to describe. A further difficulty is due to the co-presence of water and ice-particles along the path.

The dependence of the measured XPD in circular polarization on copolar attenuation has been found experimentally at 50 GHz (Italsat experiment) to follow the linear relationship [37]:

$$XPD = 0.5 \cdot CPA - 33 \tag{2}$$

This simple model takes into account both rain and ice effects, but it should be validated at higher frequencies. In fact, similarly to attenuation, also XPD worsens dramatically with the increase in frequency. If the model is confirmed at W band, it clearly appears that ice XPD is the critical issue for low margin systems since during rainy periods the system is probably already in outage. On the other hand, for gateways with high availabilities, it is rain XPD that can have an impact when attenuation is close to the system fade margin.

The higher the carrier frequency, the larger is the bandwidth available for data transmission (several gigahertz in W band). This aspect inevitably poses the problem of an accurate identification of the channel transfer function in order to highlight any possible limitation due to channel dispersion. No definite information specific for the application envisaged in this work is available in the open literature, but according to the authors' experience [38], non-marginal impact on the channel dispersion at such high frequency and large bandwidth could be expected because of the multiple scattering effects occurring during rain.

5. SYSTEM DESIGN CONSIDERATIONS

The different contributions separately discussed in the previous sections have been summed up to give the CCDF of total attenuation at Spino d'Adda (37.7° elevation angle) as shown in Figure 8 for the
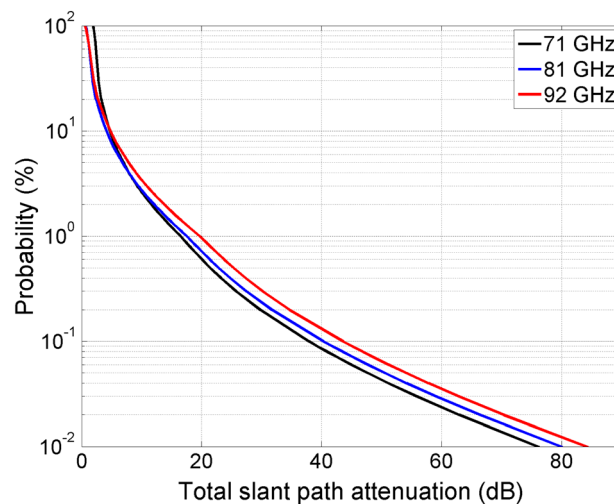
Figure 8. Complementary cumulative distribution functions of total attenuation at 71 (black line), 81 (blue line) and 92 GHz (red line) for the site of Spino d'Adda, Italy, along a 37.7° slant path (prediction using ITU-R models except for rain attenuation where the SC EXCELL model has been used).

frequencies of 71, 81 and 92 GHz. Gases, clouds and scintillation attenuations have been calculated according to the models currently recommended by the ITU-R, whilst rain attenuation has been calculated using the SC EXCELL model. The different contributions have been merged according to the formula provided by ITU-R in recommendation P.618-10 [19]:

$$A_T(p) = A_G(p) + \sqrt{[A_R(p) + A_C(p)]^2 + A_S^2(p)} \qquad (3)$$

where the attenuations due to gases (A_G), rain (A_R), clouds (A_C) and scintillations (A_S) are considered at the same probability level p. At W band, the 10 and 40 dB attenuation thresholds, taken as reference for our discussion, are exceeded for 3–4% of the yearly time (around 300 h/year) and 0.1% of the yearly time (around 10 h/year) and present the reasonable 'amount' of total tropospheric attenuation to be counteracted by the very small aperture terminals and gateways.

It follows that, being the margins required to guarantee very high system availability almost beyond the possibility offered by the current technology and, in any case, uneconomical to be implemented, the use of smart countermeasures is essential. Accordingly, several FMTs have been devised in the last years to make easier the migration towards higher frequency bands in satellite telecommunication systems. These techniques can be classified in two groups: the ones relying on meteorological properties, such as the spatial and temporal decorrelation of the atmospheric attenuation caused by meteorological phenomena (e.g. rain [39]), as well as the instantaneous frequency scaling techniques, and those more related to communication, based on the dynamic selection of the transmission/ modulation coding pair and/or the data rate control strategy to directly mitigate atmospheric propagation impairments. In the following, we briefly discuss the techniques of the first group.

On one side, considering the low spatial and temporal variability of the non-precipitating atmosphere (this statement is strictly true for oxygen and water vapour and to a lesser extent for clouds), its cumulative effect (not very large, by the way) does not benefit from the use of FMTs and has to be compensated by increasing the static margin (larger antennas, extra power of the transmitter, and so on). On the other side, in order to counteract rain attenuation above the Ka band and achieve high availability using a fixed margin, the following FMTs can be considered:

(i) On the basis of measurements and simulations up to V band, a conventional (two-site) spatial diversity scheme would allow a theoretical relative percentage gain up to 60% (an experimental characterisation in W band is highly desirable to confirm this figure).

(ii) Power control is rather simple to implement but also very effective to control uplink power after appropriate estimation (from measurements at the downlink frequency) of the actual fade suffered by the signal.

(iii) At the user side, for which low availability terminals (i.e. relatively low levels of attenuation) and lower operational frequency are foreseen, a smart system based on the use of an on-board reconfigurable antenna front-end can be envisaged.

In fact, because of the localized nature of most meteorological phenomena such as rain, adverse propagation conditions do not occur simultaneously across the whole area served by the satellite system, but it is very likely that only a small fraction of the service area is affected by severe fading. A reconfigurable antenna able to spatially rearrange the power distribution according to the actual time-variant propagation needs could be the appropriate answer to this problem. Preliminary results from simulations at Ka band have shown that an adaptive gain (similar to the one used to indicate the performance of site diversity) greater than 2 dB can be expected [40].

6. CONCLUSIONS

This contribution summarizes the impact of the atmosphere on radio waves with operational frequency in the W band. Specifically, the attenuation contributions due to gases, clouds and rain have been separately illustrated, as well as the impact of scintillation and depolarization (being ice depolarization the critical issue for low margin systems).

Results show that the fade levels to be counteracted by high availability systems (but in some cases also by low availability systems) can be so high that the classical approach for system design based on fixed power margin is no longer applicable, and adequate FMTs are required to achieve the desired QoS.

It is shown that the prediction of the propagation impairments under non-rainy conditions can be accurately carried out also in the W band, by means of state-of-the-art models, which rely on solid physical bases, even if further validations are desirable. On the other hand, much work is still needed to develop and validate rain and cloud attenuation, depolarization and scintillation prediction models. Specifically, regarding rain attenuation, the most critical point is how to correctly model the year-to-year variability of the rain rate CCDF required as input to any rain attenuation model. As for scintillations, though their impact in terms of attenuation is definitely lower than the one due to rain, for low-margin systems at low elevation angle, they have to be duly taken into account, also because of their possible detrimental interference with tracking systems or fade mitigation techniques. In addition, an experimental characterisation of FMTs, like site-diversity, adaptive coding, uplink power control or on-board resource reallocation, is needed because of the combination of effects of various atmospheric components, which are poorly characterised at W band. At the moment, only physically based models are expected to be suitable for application in the W band, but also in this case, specific tests are still required. Indeed, nowadays only measurements up to 50 GHz are available to test the models' prediction accuracy because the extrapolation to higher frequency bands is definitely critical, and there is an urgent need for new propagation satellite experiments in the W band properly designed in order to provide information on path attenuation at multiple frequencies, as well as depolarization and scintillation in different sites, together with ancillary radiometric measurements. Also, theoretical studies aimed at developing advanced space-time attenuation series synthesisers should be strongly encouraged.

REFERENCES

1. Vidal O, Verelst G, Lacan, J, Alberty E, Radzik J, Bousquet M. Next generation high throughput satellite system, *IEEE First AESS European Conference on Satellite Telecommunications (ESTEL)*, 1–7, 2–5 Oct. 2012, Rome, Italy.
2. Kyrgiazos A, Evans B, Thompson P, Jeannin N. Gateway diversity scheme for a future broadband satellite system, *The 6th Advanced Satellite Multimedia Systems Conference (ASMS 2012)* 2012; 363–370.
3. Mikkonen P. Modern 60 GHz radio link. *29th European Microwave Conference* 1999; 83–86.
4. Timms G, Kvicera V, Grabner M. 60 GHz band propagation experiments on terrestrial paths in Sydney and Praha. *Radioengineering* 2005; **14**(4): 27–32.
5. Ueba M, Miura A, Kitazawa S, Saito S, Ohira T. Feasibility Study on Millimetre Wave Multi-Gigabit Wireless LAN System, *37th European Microwave Conference* 2007; 688–691.
6. Capsoni C (editor). Assessment of propagation effects in the W frequency bands for space exploration. Final Report of the ESA/ESTEC Contract No. 21317/07/NL/HE, 2011.
7. Capsoni C (editor). Verification of propagation impairment mitigation techniques. Final Report of the ESA/ESTEC Contract No. 20887/07/NL/LvH, 2011.
8. Riva C, Capsoni C, Luini L, Luccini M, Nebuloni R, Martellucci A. W-band atmospheric radiowave propagation - a challenge for satellite TLC systems, *The 6th Advanced Satellite Multimedia Systems Conference (ASMS 2012)* 2012; 355–362.
9. International Telecommunication Union. Attenuation by atmospheric gases, recommendation ITU-R P.676-9. Geneva, 2012.
10. International Telecommunication Union. Water vapour: surface density and total columnar content, recommendation ITU-R P.836-4. Geneva, 2009.
11. International Telecommunication Union. Fascicle concerning the statistical distributions of integrated water vapour and liquid water contents given in recommendations ITU-R P.836-4 and ITU-R P.840-4. Document 3J/TEMP/48-E. http://www.itu.int/ITU-R/index.asp?category=study-groups&rlink=rwp3j-fascicles&lang=en, January 2013.
12. ERA: ECMWF re-analysis project report series, '*ERA-40 Archive*', December 2002, European Centre for Medium-Range Weather Forecasts
13. Riva C (editor). Characterisation and modelling of propagation effects in 20–50 GHz band. Final Report of the ESA/ESTEC Contract No. 17760/03/NL/JA, 2006.
14. Liebe HJ, Manabe T, Hufford GA. Millimeter-wave attenuation and delay rates due to fog/cloud conditions. *IEEE Trans Antennas and Propagion* 1989; **37**(12):1617–1623.

15. Liebe HJ, Hufford GA, Cotton MG. Propagation modeling of moist air and suspended water/ice particles at frequencies below 1000 GHz, *AGARD 52nd Spec. Meeting EM Wave Propag. Panel* 1993; 3.1–3.10.
16. Rosenkranz P. Water vapor microwave continuum absorption: a comparison of measurements and models, *Radio Sci* 1998, **33**(4): 919–928.
17. Capsoni C. et al ESTEC 21317 Final report 'Assessment of propagation effects in W bands for space exploration' May 2013.
18. Poiares Baptista JPV. Precipitation, clouds and other related Non-refractive effects. Final Report of COST Action 255. ESA Publication Division: Noordwijk (The Netherlands); Ch. 3.2.
19. International Telecommunication Union. Propagation data and prediction methods required for the design of Earth-space telecommunication systems, recommendation ITU-R P.618-10. Geneva, 2009.
20. International Telecommunication Union. Attenuation due to clouds and fog, recommendation ITU-R P.840-5. Geneva, 2012.
21. Salonen E, Uppala S. New prediction method of cloud attenuation, *Electron Lett* 1991; **27**(12):1106–1108.
22. Mattioli V, Basili P, Bonafoni S, Ciotti P, Westwater E.'Analysis and improvements of cloud models for propagation studies' Radio Science, vol. **44**, 2009
23. International Telecommunication Union. Specific attenuation model for rain for use in prediction methods, recommendation ITU-R P.838-3. Geneva, 2005.
24. Thurai M, Bringi VN. Drop axis ratios from 2D video disdrometer. *J Atmos Oceanic Technol* 2005; **22**:966–978.
25. Uzunoglu NK, Evans BG, Holt A-R. Scattering of electromagnetic radiation by precipitation particles and propagation characteristics of terrestrial and space communication systems. *Proc Ins Electr Eng* 1977; **124**(5):417–424.
26. International Telecommunication Union. Characteristics of precipitation for propagation modelling, recommendation ITU-R P.837-6. Geneva, 2012.
27. http://www.itu.int/ITU-R/index.asp?category=study-groups&rlink=sg3-dtbank-dbsg3&lang=en, January 2013.
28. Capsoni C, Luini L, Paraboni A, Riva C, Martellucci A. A new prediction model of rain attenuation that separately accounts for stratiform and convective rain. *IEEE Trans Antennas Propag* 2009; **57**(1):196–204.
29. Luini L, Capsoni C. The SC EXCELL model for the prediction of rain attenuation on terrestrial radio links. *Electron Lett* 2013; **49**(4):307–308.
30. Capsoni C, Luini L. A physically based method for the conversion of rainfall statistics from long to short integration time. *IEEE Trans Antennas Propag* 2009; **57**(11):3692–3696.
31. Aris NAM, Luini L, Din J, Lam HY. 1-Minute integrated rain rate statistics estimated from tropical rainfall measuring mission data. *IEEE AntennasWireless Propag Lett* 2013; **12**:132–135.
32. Van de Kamp MMJL, Riva C, Tervonen JK, Salonen ET. Frequency dependence of amplitude scintillation. *IEEE Trans Antennas Propag* 1999; **47**(1):77–85.
33. Tatarskii VI. Wave Propagation in a Turbulent Medium. Mc Graw-Hill: New York, 1961.
34. Matricciani E, Riva C. 18.7 GHz tropospheric scintillation and simultaneous rain attenuation measured at Spino d'Adda and Darmstadt with Italsat. *Radio Sci* 2008; **43**:RS1013, doi:10.1029/2007RS003688.
35. Filip M, Vilar E. Optimum utilization of the channel capacity of a satellite link in the presence of amplitude scintillations and rain attenuation. *IEEE Trans Commun* s; **28**:1958–1965.
36. Arbesser-Rastburg BR, Paraboni A. European research on Ka-band slant path propagation. *Proc IEEE* 1997; **85**(6): 843–852.
37. Paraboni A, Martellucci A, Capsoni C, Riva C. The physical basis of atmospheric depolarization in slant paths in the V band: theory, Italsat experiment and models. *IEEE Trans Antennas Propag* 2011; **59**(11):4301–4314.
38. Capsoni C, Mauri M, Paraboni A. Theoretical determination of the effects of multiple scattering by hydrometeors in monopulse systems at millimeter wavelengths. *Radio Sci* 1982; **17**(6):1598–1606.
39. Luini L, Capsoni C. The rainfall spatial correlation of rain over Europe investigated through the statistical dependence index. *Electron Lett* 2013; **49**(3):230–231.
40. Resteghini L, Capsoni C, Nebuloni R, Gabellini P, Maggio F, Martellucci A, Rinous P. Effect of non-ideal components on the performance of a reconfigurable on-board antenna for broadcasting applications, *EuCAP 2012* 2012.